cGAS-STING Signaling as a Therapeutic Target for Pediatric High-Grade Glioma

By

William Hawkins

BS, Bridgewater State University, 2020

Thesis

Submitted in partial fulfillment of the requirements for the Degree of Master of Science in the Graduate Program of Biotechnology at Brown University

PROVIDENCE, RHODE ISLAND

April 2025

AUTHORIZATION TO LEND AND REPRODUCE THE THESIS

As the sole author of this thesis, I authorize Brown University to lend it to other institutions for the purpose of scholarly research.

Date 4/28/2025

DocuSigned by:
William Hawkins
43E6D97D84A54FC...

William Hawkins, Author

I further authorize Brown University to reproduce this thesis by photocopying or other means, in total or in part, at the request of other institutions or individuals for the purpose of scholarly research.

Date 4/28/2025

DocuSigned by:
William Hawkins
43E6D97D84A54FC...

William Hawkins, Author

This thesis by William Hawkins is accepted in its present form by the Graduate Program in Biotechnology as satisfying the thesis requirements for the degree of Master of Science

Date 4/28/2025 Signature: DocuSigned by: Sean Lawler 6A2688E8BBC5498...

Dr. Sean Lawler, Advisor

Date 4/29/2025 Signature: DocuSigned by: Elena Oancea E2ECAF3DD9FF4C7...

Dr. Elena Oancea, Reader

Date 4/28/2025 Signature: DocuSigned by: EDITH MATHIOWITZ E063C09A6ABC428...

Dr. Edith Mathiowitz, Reader

Approved by the Graduate Council

Date _____ Signature: _____

Dr. Thomas Lewis, Dean of the Graduate School

Acknowledgments

First and foremost, I would like to express my deepest gratitude to Dr. Sean Lawler for his unwavering support throughout my master's program and during the year prior when I had the privilege of working with him as a research assistant. Over the past three years, Sean has continually pushed, encouraged, and inspired me, fostering both my growth as a researcher and my confidence in my work. I will always be grateful for the invaluable opportunities I have had as part of the Lawler Lab.

I am also incredibly thankful to my fellow Lawler Lab members—Pippa, Andy, Noe, Jasmine, Michelle, Sandy, and Jorge—who have not only guided me through every step of my research but have also become wonderful friends. Your support, collaboration, and camaraderie have made this experience both enriching and enjoyable.

Beyond the lab, I am fortunate to have an amazing group of friends—Reid, Chris, Morgan, Kacie, Ali, and Lyndsey—who have provided me with a much-needed escape from work, offering laughter, relaxation, and encouragement. Your friendship has been invaluable in making this journey far less stressful.

Finally, I am profoundly grateful to my parents for their unwavering encouragement. To all who have supported me along this journey—thank you. This achievement would not have been possible without you.

Table of Contents

Table of Figures

Table of Tables

Abstract of cGAS-STING Agonists as a Therapeutic Target for Pediatric High Grade Glioma by William Hawkins, SCM, Brown University, April 2025

Objective: Pediatric high-grade gliomas are among the most aggressive pediatric malignancies, associated with poor prognosis and limited therapeutic options. This study evaluates the therapeutic potential of ADU-S100, a cGAS-STING agonist, aiming to enhance innate immune responses in these typically immunologically cold tumors.

Methods: Patient-derived pHGG cell lines were treated *in vitro* with the cGAS-STING agonist ADU-S100. The activation of the cGAS-STING pathway was evaluated using Western blot analysis, while the viability of tumor cells post-treatment was measured using CellTiter-Glo assays. The functional response of the pathway was further confirmed by quantifying secretion of canonical STING-induced cytokines C-C Chemokine Ligand 5 (CCL5) and interferon gamma-induced protein 10 (CXCL10) via ELISA. Following the identification of a responsive cell line, co-culture experiments were conducted with peripheral blood mononuclear cells (PBMCs) at various ratios and ADU-S100 concentrations to model immune-mediated tumor cell killing. Finally, to establish an *in vivo* disease model, a murine-derived H3K27M mutant cell line was intracranially implanted in mice for validation and future therapeutic testing.

Results: cGAS-STING signaling pathway components were detected in pHGG cell lines by western blot. ADU-S100 treatment resulted in robust activation of the cGAS-STING pathway in the SU-DIPG-36 cell line, demonstrated by increased secretion of CCL5 and CXCL10, indicative of a type I interferon response.ADU-S100 treatment resulted in a decrease in viability for SU-DIPG-4 and HCMEC cells. However, co-culture experiments did not demonstrate significant immune-mediated tumor cell death, irrespective of ADU-S100 dosage or PBMC-to-tumor-cell

ratio. An *in vivo* murine model of H3K27M-mutant pHGG was successfully established, confirmed by intracranial tumor growth expressing the H3K27M mutation.

Conclusions: This study identifies SU-DIPG-36 cells as a responsive pHGG cell line to ADU-S100, and SU-DIPG-4 cell lines as having a significant reduction in ATP post treatment with ADU-S100, providing critical models to further investigate cGAS-STING activation and its potential as a biomarker-driven therapeutic approach. Although the co-culture assay highlighted challenges in modeling immune-mediated cytotoxicity *in vitro*, the successful development of a relevant murine tumor model offers valuable opportunities for future preclinical therapeutic investigations.

Chapter 1: Introduction

Pediatric High-Grade Gliomas

Pediatric brain tumors constitute the most common solid malignancies in children, with pHGG representing approximately 8–12% of these cases (1). pHGG are broken down into four subsets as follows: Diffuse midline glioma H3K27 Mutant (DMG), Diffuse Hemispheric Glioma G34R/V mutant (DHG), Diffuse pediatric type high-grade glioma H3 wildtype and IDH wildtype, and infant type hemispheric glioma (2). Of interest in these studies are the G34R/V Diffuse Hemispheric Glioma and the H3K27 Mutant Diffuse midline Glioma. There is currently no universally established standard of care for DHG; however, most patients undergo surgical resection when feasible, followed by radiation therapy. Many patients also undergo chemotherapy with Temozolomide, a DNA damaging drug, being the most commonly used agent (4). The median overall survival for DHG patients is approximately 17.3 months, with a median age at diagnosis of 15 years old (4). The standard of care for DMG involves radiation therapy alone, as tumor location within vital brainstem structures such as the pons precludes safe surgical resection (Figure 1). Alongside radiation therapy, DMG patients commonly receive Dexamethasone, a corticosteroid administered to manage cerebral edema (2). Median survival rate for DMG is 10 months and is diagnosed most commonly between the ages of 5-7 (2).

In 2021, the World Health Organization (WHO) reclassified pediatric gliomas, formally distinguishing them from adult high-grade gliomas such as glioblastoma based primarily on

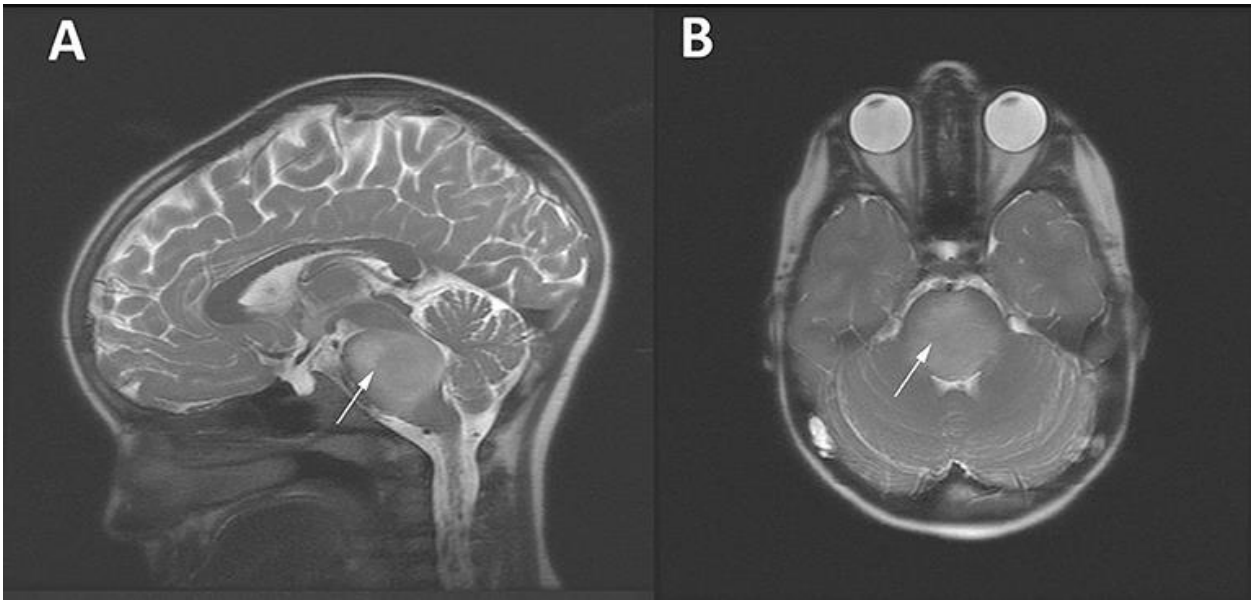

Figure 1 **MRI scan of DMG** : A sagittal orientation of DMG scan white arrow indicates area of tumor. B Axial orientation of the same DMG tumor white arrow indicates area of tumor. (5)

molecular characteristics. Molecular markers were first used to define these tumors as opposed to the classical histological approach in 2021(6). H3K27M is a mutation that defines DMG and is implicated in tumorigenesis The H3K27M mutation occurs on two distinct histone variants, H3.3 and H3.1. H3.3 is the more common variation and is a missense mutation that alters the protein coding sequence resulting in substitution of lysine at position 27 for a methionine on histone 3.3. H3.1 mutations substitute the lysine at position 27 for a methionine on histone 3.1.(6). Both mutations result in histone hypomethylation, causing transcriptional deregulation and promoting tumorigenesis (6,7). G34R/V mutations characterize DHG and involve the substitution of glycine at position 34 with arginine or valine on histone 3.3. This change results in greater methylation of other sites on Histone 3.3 that affect DNA repair systems resulting in tumorigenesis (7).

In vitro DMG models predominantly consist of patient-derived cell lines established by the Monje lab at Stanford University. These are patient derived cell lines originating in the Pons. In our studies we will focus on SU-DIPG-XXXVI (DIPG-36) and SU-DIPG-IV (DIPG-4) cell

lines. Both of these are known to be H3.1 K27M mutants (9,10). To model DHG *in-vitro* KNS42 cells were used. KNS42 is a mutant G34V patient derived cell line (8).

These tumors carry with them a dismal prognosis and a strong need for new therapeutic strategies. This study aims to improve therapeutic options for these malignancies by evaluating ADU-S100, a cyclic GMP-AMP synthase–stimulator of interferon genes (cGAS-STING) agonist.

Immunotherapies in development for pHGG

With the current standard of care proving ineffective at prolonging long-term survival, many groups have begun exploring immunotherapies in hopes of finding more effective treatment for these debilitating diseases. The front runner of these therapies in DMG is ganglioside GD2 (GD2) chimeric antigen receptor (CAR) T cells. GD2 is a glycolipid that under healthy conditions is responsible for maintaining neuronal tissue and resides on the cell surface (10). GD2 is highly expressed on the surface of tumor cells and within the tumor microenvironment, making it an ideal candidate for CAR-T cell therapy. Its accessibility to the T-cell receptor complex further enhances its therapeutic potential (11). Preclinically GD2 CAR-T cells were shown to be highly effective in xenograft models of DMG offering long term survival methods across three cohorts of 22 mice (12). In the clinic, GD2 CAR-T cells are now in a phase I clinical trial. In this clinical trial, GD2-targeted CAR-T cells were delivered via intracerebroventricular (ICV) infusions. Patients were then monitored for any adverse events as well as disease progression via MRI and patients that responded were given subsequent doses through the same route of administration (13).

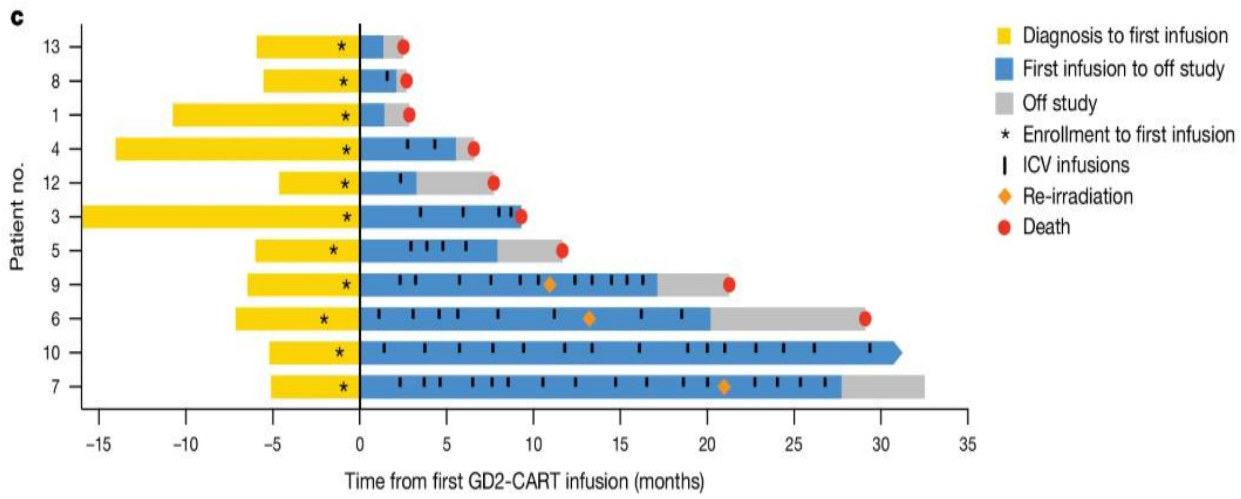

Figure 2 **GD2 CAR-T cell Phase 1 trial**: Swimmer Plot from GD2 CAR-T cell trial showing 11 trial participants, the bar in yellow represents the time since diagnosis until first infusion, each hatch mark represents an ICV infusion, a red circle represents death, and gray bars represent time off study Participants remained on study until they were no longer responsive to GD2 CAR-T cell therapy. (13)

Figure 2 summarizes outcomes from the initial 13 patients enrolled in the phase 1 clinical trial, highlighting extended survival times beyond standard-of-care expectations in several patients. Along with CAR-T Cell therapy there have been at least six clinical trials testing the effectiveness of immune checkpoint blockade inhibitors for DMG including anti-PD1 and anti-CTLA4. None of those trials had a convincing positive impact on overall survival. The unique epigenetic landscape of DMG makes the tumor microenvironment resistant to immunotherapy. This resistance is characterized by low T-cell infiltration, reduced inflammatory cytokine production, and elevated CTLA-4 expression, which collectively promote T-cell exhaustion (14).

In H3G34R/V DHG, a phase I clinical trial is investigating peptide pulsed dendritic cell vaccines using a neoantigen of H3G34R/V DHG to train the patient's own immune system to recognize

H3G34R/V DHG cells and eliminate the tumor (NCT06342908). No results have been reported as the trial is still ongoing. In preclinical studies, researchers from the University of Michigan demonstrated prolonged survival in genetically engineered mouse models of H3G34-mutant DHG following treatment with a STING agonist combined with radiotherapy and inhibition of poly (ADP-ribose) polymerase (PARP), a regulator of DNA damage repair (15).

Given the increasing focus on immunotherapies in clinical trials for pHGG and the potential of cGAS-STING agonists as standalone or combination treatments, we sought to investigate the mechanism of action and therapeutic efficacy of the cGAS-STING agonist ADU-S100. This work aims to clarify its potential role in improving clinical outcomes for pediatric glioma patients.

cGAS-STING

The cGAS-STING pathway is a highly conserved cytosolic double-stranded DNA (dsDNA) sensing mechanism, which triggers type I interferon and inflammatory cytokine responses (16). Cyclic GMP-AMP synthase (cGAS) initiates the signaling cascade upon detection of cytosolic double-stranded DNA, typically associated with viral infections. However, cytosolic DNA can also result from genomic instability during cancer progression or DNA damage induced by irradiation (17). Activated cGAS synthesizes a messenger molecule known as cyclic guanosine monophosphate–adenosine monophosphate (cGAMP). cGAMP binds to and activates Stimulator of Interferon Genes (STING) which is present on the endoplasmic reticulum membrane. Upon activation, STING undergoes phosphorylation and translocates to the Golgi apparatus. Following STING activation, Tank Binding Kinase 1 (TBK1) is phosphorylated. Activated TBK1 then phosphorylates the transcription factors Interferon Regulatory Factor 3 (IRF3) and Nuclear Factor-κB (NF-κB). These transcription factors drive the production of type I interferon and

inflammatory cytokines, notably interferon gamma-induced protein 10 (CXCL10) and C-C Chemokine Ligand 5 (CCL5) as shown in figure 3 (18,19).

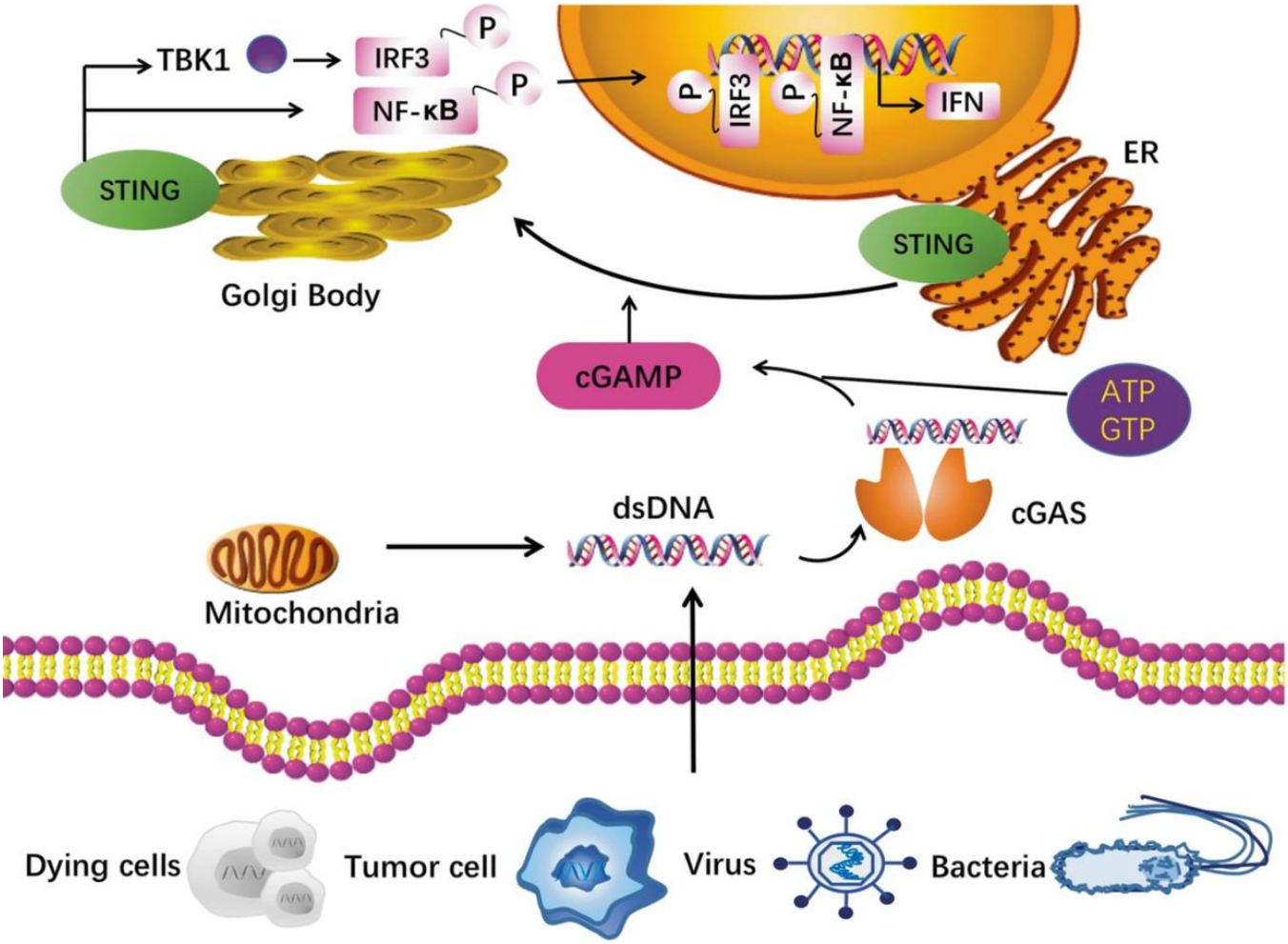

Figure 3 **cGAS-STING pathway**: A depiction of the cGAS-STING pathway where dsDNA is recognized by cGAS which is then converted to cGAMP that activates STING which is translocated from the ER to the Golgi Body before TBK1 activation followed by IRF3 and NF-κB. which are transcription factors that drive a type I interferon response (23).

In cancer, the cGAS-STING pathway is particularly attractive as a therapeutic target because proper activation promotes recruitment of immune cells to tumor sites, facilitating immune-mediated recognition and clearance of malignant cells. Beyond this dsDNA is most likely to be present as a byproduct of many cancer treatments like radiation that causes damage to chromatin,

or chemotherapies that disrupt cells regular function, or be a product of the cancerous growth linked to prolonged replication and resistance to senescence (17).

Chronic activation of the cGAS-STING pathway can also promote tumorigenesis through non-canonical NF-κB signaling (17). Non-canonical NF-κB signaling, first described in 2001, drives chronic inflammation and dendritic cell exhaustion, and enhances infiltration of regulatory T cells (Tregs) into the tumor microenvironment, impairing effective anti-tumor immune responses (17,20). This signaling pathway occurs when there is high chromosome instability in the tumor cells, and aids the tumor in evading the immune system (17).

***In Vivo* models of pHGG**

The *in vivo* model used in this study is a H3.3 K27M, tumor protein 53 (p53) loss of function mutant, platelet-derived growth factor receptor alpha (PDGFRA) missense mutation aspartic acid at position 842 is substituted with a valine (D842V) identified as KPD (21). This combination of mutations was induced via *in-utero* electroporation (IUE) , a system whereby mutations are introduced *in-utero* to neural stem cells of mice (21). These are common mutations seen alongside H3K27M mutations in DMG and the goal of introducing them was to elucidate whether the H3K27M mutation alone was enough to cause oncogenesis. This group found that these tumors needed a second mutation in order for the tumor to progress. This model was chosen because of its low survival time and invasive phenotype that closely resembles human disease (21).

Prior work in the Lawler Lab

In preclinical studies of glioblastoma (GBM), an adult high-grade glioma, the STING agonist ADU-S100—a biosimilar to cGAMP—has emerged as a promising therapeutic candidate (22). Patient-derived and commercially available human GBM cell lines were used alongside mouse GBM cell lines CT2A and GL261 as *in vitro* models. An *in vitro* co-culture model was established using G9 GBM cells and peripheral blood mononuclear cells (PBMCs), as illustrated in Figures 4C and analyzed in 4D (22). This co-culture model involved seeding 5,000 G9 cells

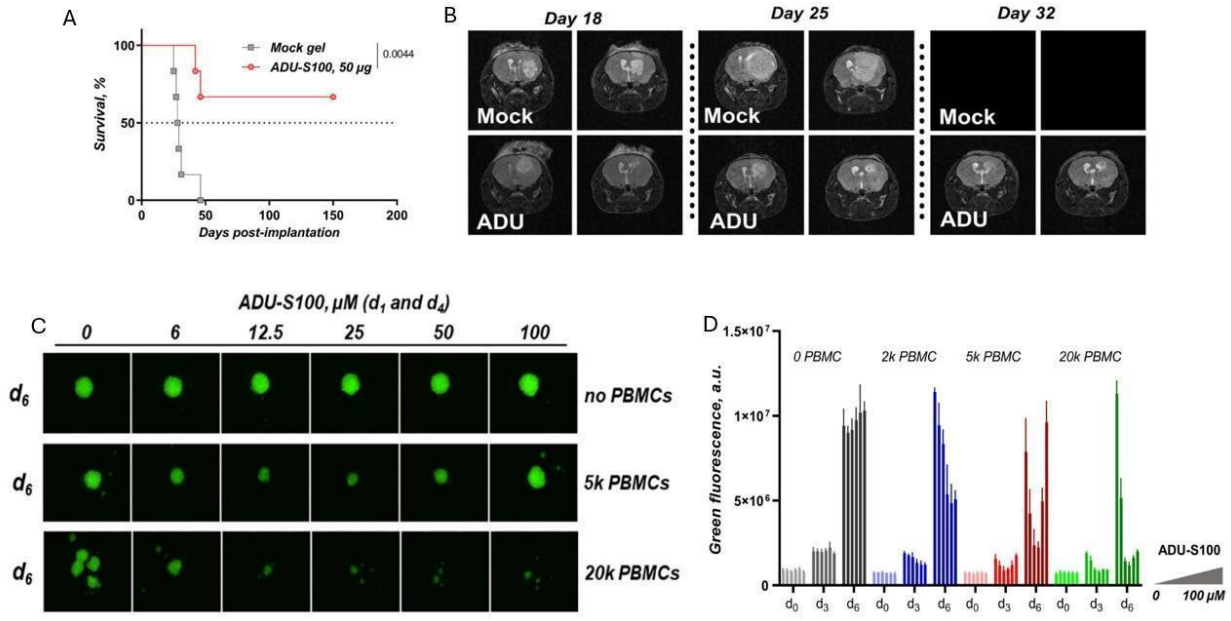

Figure 4 Response to ADU-S100 in vivo and in-vitro:4a survival curve showing untreated and treated mice with ADU-S100 cross-linked hydrogel using a GL261 tumor model. 4B MRI images of ADU-S100 vs mock hydrogel from this study showing a decrease in tumor volume. 4C IF images of fluorescent G9pCDH cell lines at day 6 of co culture. 4D quantification of Green fluorescence measured in PBMC co culture assay.(22)

treated with varying concentrations of ADU-S100 and different ratios of PBMCs. In vivo studies demonstrated increased survival in mice bearing GBM tumors treated with ADU-S100 cross-

linked hydrogels (Figure 4A). Although data from the CT2A model are not included in this figure, a significant increase in survival were also observed. However, treatment with ADU-S100 alone did not result in tumor eradication.

Given the promising results of ADU-S100 in adult GBM models showing enhanced immune responses and improved survival, we hypothesized ADU-S100, a cGAS-STING agonist, could be used to effectively stimulate the cGAS-STING pathway, resulting in immune mediated cell death of the tumor cells and opening the door to new effective therapeutics. Here we aimed to better understand if the pathway was functional in patient derived DMG cell lines SU-DIPG4, and SU-DIPG 36 and the DHG cell line KNS-42. We did this while simultaneously trying to establish a mouse model of DMG to be used in future studies.

Chapter 2: Methods

Cell Culture

Cells were kept at 37 °C, at 5% CO2 while being cultured. KNS-42 cells (Chiocca lab, Brigham and Women's hospital-Harvard University) and were grown in DMEM-F12 (Thermo #11320033) supplemented with 50mL of fetal bovine serum, and 5mL of penicillin/streptomycin (Thermo #15140-122). SU-DIPG-36 and SU-DIPG-4 cell lines (Tapinos lab, Brown University originally from Monje Lab, Stanford University) and were grown in a media made of 237.5mL of Neurobasal A media (Thermo #10888-022) and 237.5 mL DMEM F12 (Thermo #11320033) that is supplemented with 5mL HEPES buffer solution (Thermo #15630-080), 5mL MEM sodium pyruvate solution (Thermo #11360-070), 5mL MEM non-essential amino acids (Thermo #11140-050), 5mL Glutamax supplement (Thermo #35050-061) and 5mL antibiotic antimycotic (100x) liquid (Thermo #15240-096). 50mL of this media is then transferred to a 50mL conical before adding 50µL of heparin (Stemcell #07980), 1mL of B27 (Thermo #12587-010), 10µL of EGF and FGF (Shenandoah Biotech #100-26 and 100-146) for a final concentration of 10µg/mL, and 50µL of PDGF AA and PDGF BB (Shenandoah Biotech #100-16 and #100-18) for a final concentration of 10µg/mL. KPD mouse cell lines (Pathania lab Cambridge University) were grown in Neurocult mouse media (Stemcell #05702) plus 10µg/mL PDGF-AA, PDGF-BB, EGF and FGF (Shenandoah Biotech #100-16, #100-18, #100-26,100-146) Human cerebral microvascular endothelial cells (HCMEC) (Millipore Sigma #SCC066) were grown in Sciencell ECM media (Sciencell #NC9692874).

Viability Assay

Cells were grown to 80% confluency before being harvested and seated in 200µL of media at 1500 cells per well in a black 96 well flat bottom plate (Corning #3603). Cells were left overnight before adding ADU-S100 to a final concentration of 50µM. The next day radiation was administered at 2GY per day for 3 days using the Orthovoltage X-ray machine. After 5 days total viability was measured using Cell Titer Glo 2.0 (Promega #G9242) following manufacturer's instructions and quantified for luminescence signaling using a Molecular Devices Spectramax M2 Plate reader.

Western Blot

For western blotting, pHGG and HCMEC/D3 cell lines were collected in 50µL of RIPA buffer (Thermo #89900) with 1x protease and phosphatase inhibitor (Cell Signaling #5872S). Protein was quantified using Pierce BCA protein assay kit (Thermo #23227) at 562 nm absorbance on Molecular Devices Spectramax M2 Plate reader. Lysates were incubated in Laemmli sample buffer (Bio Rad #1610747) at 95°C for 5 minutes and then loaded into a 10% precast polyacrylamide gel (Bio Rad #4561033). Thermo Pageruler Plus prestained protein ladder (Thermo #26619) was used for protein identification. After the gel was run transfer of the protein to a polyvinylidene difluoride (PVDF) membrane was done with the Biorad Trans Blot Turbo Transfer system, using the mini PVDF Transfer pack (Bio Rad #1704156EDU). Membrane was then blocked in 5% milk and 1x TBST with 0.5% Tween for 1 hour while shaking at room temperature. Washes were all done in 1x TBST with 0.5% Tween. Primary antibodies were incubated in 5% BSA and 1x TBST with 0.5% Tween at 1:1000 dilution overnight at 4°C while shaking. Goat-Anti Rabbit HRP secondary (Sigma-Aldrich #401353) antibody at 1:5000 was

incubated for 1 hour at room temperature while shaking in 5% milk and 1x TBST with 0.5% tween. Blots were imaged using Super signal West Pico Plus Chemiluminescent substrate (Thermo #34577) on the Chemidoc imaging system (Bio Rad).

Table 1 Antibodies used for Western Blot and Staining

Antibody Target	Vendor and catalog number	Application and dilution
cGAS	Cell Signaling 15102S	Western Blot 1:1000
STING	Cell Signaling 13647S	Western Blot 1:1000
P-TBK1	Cell Signaling 5483S	Western Blot 1:1000
H3K27	Cell Signaling 74829S	Western Blot 1:1000
H3K27	Cell Signaling 74829S	IF staining 1:1600
Beta Actin	Cell Signaling 4967L	Western Blot 1:1000

Enzyme linked Immunosorbent Assay (ELISA)

Supernatants from SU-DIPG-36, DIPG-4, KNS-42, and HCMEC cells were collected after 24 hours of ADU-S100 treatment. CXCL10 and CCL5 were measured using Peprotech ELISA kits (#900-K39 +HRP Conjugate, and #900-K33 + HRP conjugate) and following standard protocols. In summary, 500µL of 0.50µg/mL capture antibody diluted in PBS was added to the provided ELISA plate per well before being sealed and incubated overnight at room temperature. The next day four washes were done with Peprotech wash buffer (Peprotech #900-K00) before 300µL of block buffer consisting of 1% BSA in PBS was added to the ELISA plate per well and left to incubate at room temperature for 1 hour. After incubation the plate was washed another four times with a wash buffer before standards and samples were plated in triplicate, and incubated at room temperature for 2 hours. After incubation four washes were done and detection antibody

added and left to incubate for 2 hours. After incubation four washes were done, before a horseradish peroxidase conjugate was added that has been diluted 1:2000 in diluent as stated in the Peprotech protocol and left to incubate for 30 minutes. Finally, the plate was washed four more times with a wash buffer before 100µL of Liquid substrate was added to all wells; the plate was then left to develop for 10 minutes before reading out every 5 minutes for 25 minutes to ensure maximum development. The plate was read out at 405 nm on the Molecular Devices Spectramax M2 Plate reader.

Generation of mCherry labeled SU-DIPG36 cells:

100,000 SU-DIPG-36 cells were plated in a 6 wells of a 24 well plate 24 hours prior to adding the lentivirus in 500µL of associated media.1.5µL mCherry lentivirus (Genecopeia #LP441-025) was then added to 1.5mL of media supplemented with 5µg/mL of polybrene (Millipore Sigma #TR-1003) 500 µl of this media was used to replace the media in 3 of the wells and polybrene control media was used to replace the media in 3 control wells. 24 hours after cell media was refreshed without polybrene. On Day 5 cells were visualized using the Zeiss 880 confocal microscope with the mCherry filter and mCherry positive cells were identified in experimental wells. After imaging media was refreshed and 2µg/mL of Puromycin (Fisher #A1113803) was added; cells were observed daily for 7 days for lentivirus infected cell colonies. After 7 days all cells in the experimental wells exhibited stable expression of mCherry and all cells in the control well were dead. SU-DIPG36 mCherry labeled cells were then returned to normal media conditions without Puromycin and frozen at $2.0x10^6$ cells per vial.

Co-culture models

SU-DIPG 36 cells labeled with mCherry are platted at 5000 cells/well in ultra-low attachment U bottomed black 96 well plates (Corning #4515). Cells were spun down at 200 x g for 20 minutes to create spheres and left to incubate for 48 hours. After 48 hours peripheral Blood Mononucleated cells (PBMCs) were added as well as ADU-S100 at varying concentrations. 24 hours after images were taken every other day for 5 days using the Zeiss 880 confocal microscope with the mCherry filter and mean total fluorescence is calculated using ImageJ. Images were taken at 24, 72, and 120 hours at 10x magnification.

PBMC Isolation

PBMCs were isolated using a density gradient Ficoll-Paque (Cytiva #17544602). Whole blood was obtained from the Rhode Island blood center through an agreement with the Lawler lab. Blood is plasma depleted before adding PBS for a 1:1 ratio of PBS and plasma depleted blood. This blood is then overlaid carefully on top of 15mL of Ficoll-Paque to create a clear phase separation between diluted blood and density gradient. Overlays are then spun in a centrifuge at 500 x g for 30 minutes without use of the break in the centrifuge. The buffy coat is extracted from these overlays and washed 3 times in DPBS before being frozen down at $5.0x10^6$ cells/vial. PBMC viability is confirmed post thaw with a cell count using the Countess cell counter and trypan blue.

Mouse model

C57 BL6 mice purchased at 8 weeks old from Envigo were used for the mouse model. All procedures were done following guidelines of the Institutional Animal Care and Use Committee

(IACUC) with support from the Center for Animal Resources and Education (CARE) at Brown University.

KPD Cell line implantation

KPD cells (Pathania lab Cambridge University) were cultured prior to implantation and dissociated into single cell neurospheres on day of surgery. 200,000 cells were resuspended in 3µL of sterile PBS and injected intracranially. Injections were done using a stereotaxic frame where the mouse's head was positioned using ear bars, injections were done 2mm to the right and 1 mm frontal of the bregma. Cells were injected 3mm deep at a rate of 1 µL/minute and the needle was retracted at a rate of 1 mm/min. Animals were anesthetized using isoflurane and given Lidocaine topically, as well as buprenorphine SR at 0.6mg/kg and Meloxicam ER at 5mg/kg pre-surgically. Animals were then monitored daily for three days before switching to being monitored twice a week until signs of disease progression were observed. After 51 days two mice were taken down for sectioning and staining of the brain to confirm tumor implantation was successful and tumor was continuing to express the H3K27M mutation. One mouse is still being monitored.

Immunofluorescence (IF) Staining

Sectioning of brains was done on a cryostat at 6µm thickness and frozen at -80 ℃ until staining was done by letting slides reach room temperature before a hydrophobic barrier pen was used to outline the slide to avoid runoff of reagents. Permeabilization was achieved with 0.05% Triton X-100 (Sigma #9036-19-5) after 5 minutes the TritonX-100 was removed and blocking solution was added made of 0.05% normal donkey serum (Sima #566460) in 0.01% Tween 20 in PBS (Thermo #AAJ63314K2), blocking buffer was left on samples for 1 hour at room temperature

protected from light. After one hour blocking buffer was removed and primary antibody for H3K27M (Cell signaling #74829S) was made at 1:1600 dilution in blocking buffer and added to samples, primary antibody was left on for 2 hours at room temperature protected from light. Primary antibody was then removed and slides were washed three times with PBS before secondary antibody solution was added. Secondary antibody solution was made using a 1:500 dilution of Alexa Fluor-647 donkey anti-rabbit (Thermo #A31573) and Hoechst dye at 1:2000 (Thermo #62249) in blocking buffer. Secondary antibody solution was added to samples and left to incubate at room temperature away from light for one hour. Finally, three washes were done with PBS before coverslips were mounted using Fluoromount G (Thermo #00-4958-02). Fluorescence was detected by illuminating the samples with a laser adjusting the wavelength to excite the dyes on a Zeiss LSM 880 confocal microscope at 10x magnification.

Hematoxylin and Eosin staining:

Brain sections were prepared in the same manner as IF staining, Slides were first dipped washed in tap water before being placed in a hematoxylin (Vector Laboratories #H-3502) for 2 minutes they were then washed in tap water, and before a drop of bluing reagent (Vector Laboratories # H3502) was added and left on for 10 seconds before another wash was done in tap water. 3 drops of Eosin (Vector Laboratories #H-3502) was added per section and left for 1 minutes before being washed in water followed by minute long washes in 80% ethanol, then 95% ethanol, and finally 100% ethanol. 3 rounds of Xylene baths (Vector Laboratories #H-3502) was then performed where slides were submerged in xylene for 3 minutes and then washed with tap water. Imaging was done on EVOS XL core brightfield microscope at 10x magnification.

Statistical Analyses:

All statistical analyses were performed using GraphPad-Prism software, two tailed T tests were performed for Viability data analysis. P value less than 0.05 was deemed statistically significant.

Chapter 3: Results

Effect of ADU-S100 on pHGG cell lines:

To investigate whether STING pathway components were present in pHGG cells, western blotting was performed. pHGG cell lines were lysed and protein levels of β-actin, cGAS, STING and phospho-TBK1 were measured (Figure 5). β-actin was used as a loading control. cGAS protein levels remained stable following ADU-S100 treatment in all tested cell lines. STING protein was detected in all pHGG cell lines but decreased notably in KNS-42 cells after 24 hours of treatment. DIPG-4 cells appeared to lose STING expression following treatment, but due to low overall protein recovery, this result requires confirmation. Phospho-TBK1 is used as a marker for STING activation and is present in Human cerebral endothelial cells (HCMEC), these cells are a brain endothelial cell immortalized cell line (22) that has previously been shown to have canonical activation of the STING pathway after treatment with ADU-S100 (22). P-TBK1 is present in DIPG-36 cells before and after ADU-S100 treatment but does not appear to be present in the KNS-42 cell line. The DIPG-4 cell line is excluded from this blot due to low protein levels, and no loading control is present so no changes can be detected between treated and untreated groups.

For cell viability cells were treated with 50μM of ADU-S100 or DPBS control in the same volume. Cell Titer glo is a luminescence-based assay and thus readout is relative light units (RLU). A significant reduction in DIPG-4 cell viability was observed following ADU-S100 treatment alone ($p=0.0195$) after 96 hours. This effect was further enhanced when combined with radiation therapy ($p=<0.0001$). No significant changes were observed in DIPG-36 or KNS-42 cells under identical treatment conditions. In HCMECs, this same assay was conducted and a

significant decrease (p=0.0156) in viability was only observed in the ADU-S100 and irradiated group. Irradiation was used here to mimic the standard of care therapy patients receive with pHGG and as a way to potentially enhance the effectiveness of ADU-S100 due to the larger amount of extra nuclear DNA.

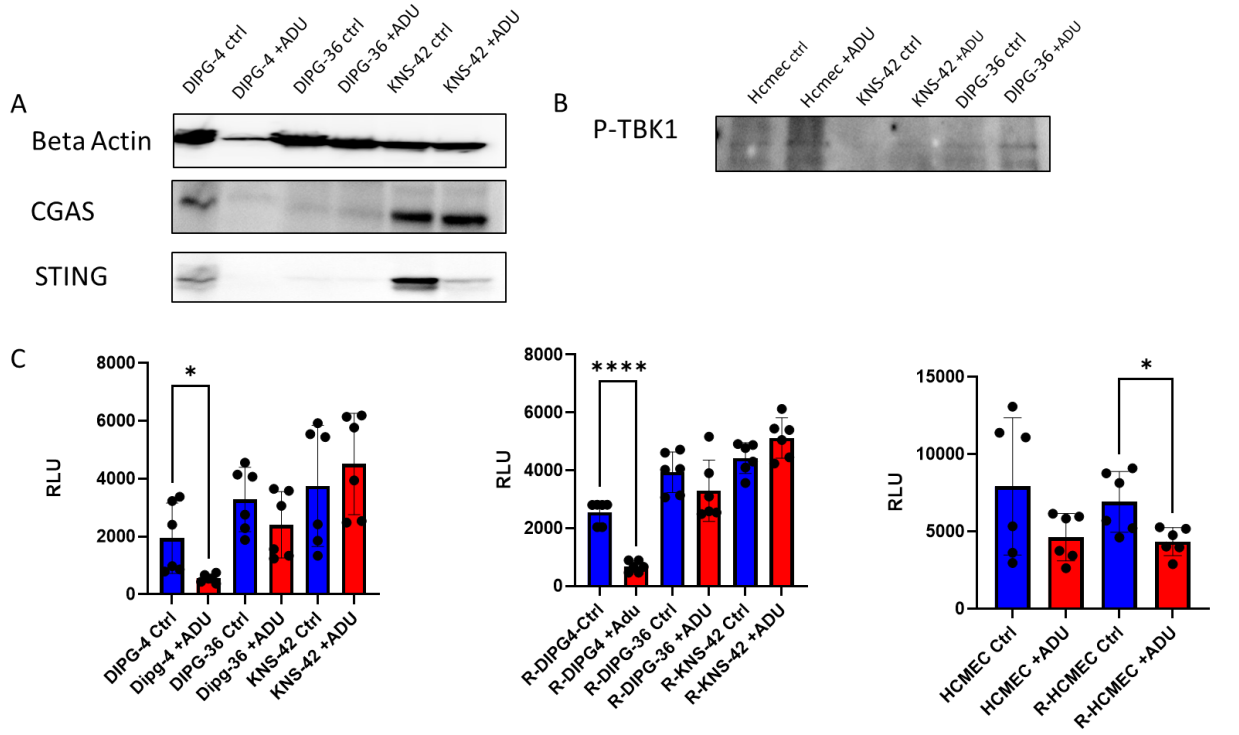

Figure 5 Effect of ADU-S100 on pHGG cell lines: A) Western blot of DIPG-4, DIPG-36 and KNS-42 cell lysates after 50 µM ADU-S100 treatment for 24 hours. Beta actin used as a loading control 3 replicates B) Western blot of Human Cerebral microvascular cells (HCMEC), KNS-42 and DIPG-36 lysates measuring phospho-TBK1 3 replicates DIPG-4 cell lysates were not included because of low protein levels 3 replicates. C) Cell viability data from Cell Titer Glo assay showing changes in viability of DIPG-4, DIPG-36, KNS-42, and HCMEC cells after 96 hours treatment with ADU-100 and Radiation. 3 technical and 2 biological replicates.

Functional Assays

Treatment with the STING agonist ADU-S100 should lead to cytokine secretion through IRF3 and NF-κB activation if the pathway is functional. Using an ELISA we measured CCL5 and CXCL10, two known products of the cGAS-STING pathway (18,19). DIPG-36, DIPG-4, and KNS-42 cell supernatants were collected after 24 hours of 50μM ADU-S100 treatment (Figure 6). DIPG-4 and KNS-42 cells showed no detectable secretion of CCL5 or CXCL10 at the 24-hour time point and were therefore omitted from Figure 6. DIPG-36 cells have nearly 1000pg/mL CXCL10 and CCL5 24 hours after ADU-S100 treatment, a significant increase compared to the control group (P=.0224, P=.0018 respectively). ELISA was completed in three technical replicates; more biological replicates are needed.

DIPG-36 cells were deemed a responder cell line because of their intact cGAS-STING pathway as evidenced by western blot analysis, and their production of CXCL10 and CCL5. DIPG-36 cells were then transfected with an mCherry lentivirus (Genecopoeia: LPP-MCHR-Lv105-025-C) to be used in the PBMC co-culture model. 5000 DIPG-36 cells were plated into a 96 well plate and allowed to form spheres for 2 days before ADU-S100 and PBMCs were added at various concentrations (Figures 7-10) to test if we could recapitulate immune mediated cell death *in vitro*. Three technical replicates were done and one biological replicate so no significance can be determined. Figure 7 shows DIPG-36 cells at day 1,3, and 5 after a control PBS treatment. We used corrected total fluorescence (CTCF) as a proxy for cell viability. Universally on day 5 there was a large reduction in fluorescence and any differences seen between day 1 and day 3 are inconsistent. Differences between PBMC ratios are also not consistent. Figure 8 Shows the assay previously described with 10 μM ADU-S100 treatment there is again a large reduction on Day 5

but changes between day 1 and day 3 are inconsistent as well. This trend continues for figure 9 and 10. Figure 11 shows the co-culture images taken where you can see the large drop off at day 5 regardless of experimental condition. Significant reduction in fluorescence by day 5 across all conditions suggests technical limitations, such as compromised spheroid integrity, PBMC viability, or media exhaustion. Future experiments would benefit from improved culture conditions, additional viability assays, or alternate imaging methods to better assess true therapeutic effects.

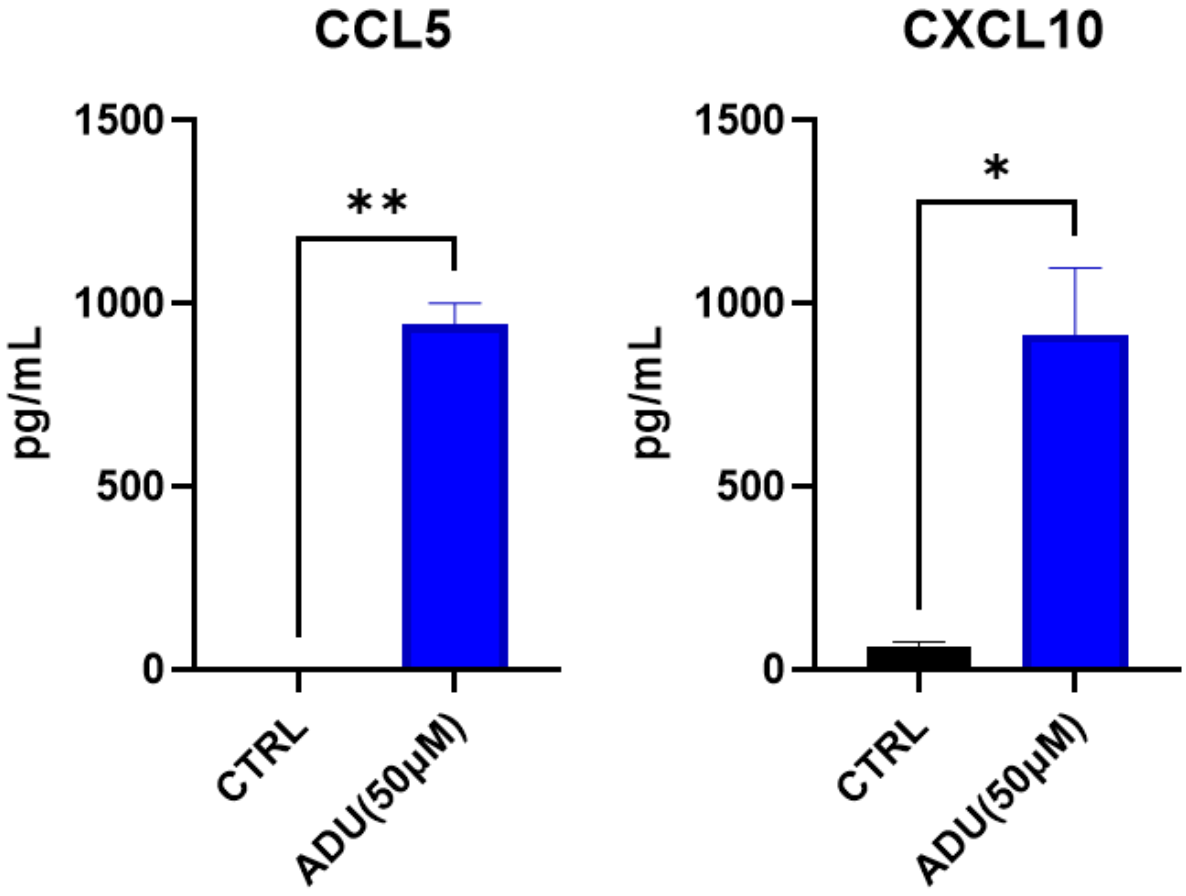

Figure 6: ELISA measuring CXCL10 and CCL5 in pg/ml: DIPG–36 cell line supernatant was measured for CCL5 and CXCL10. KNS-42 and DIPG-4 supernatants were also measured but no CCL5 and CXCL10 was detected n=3.

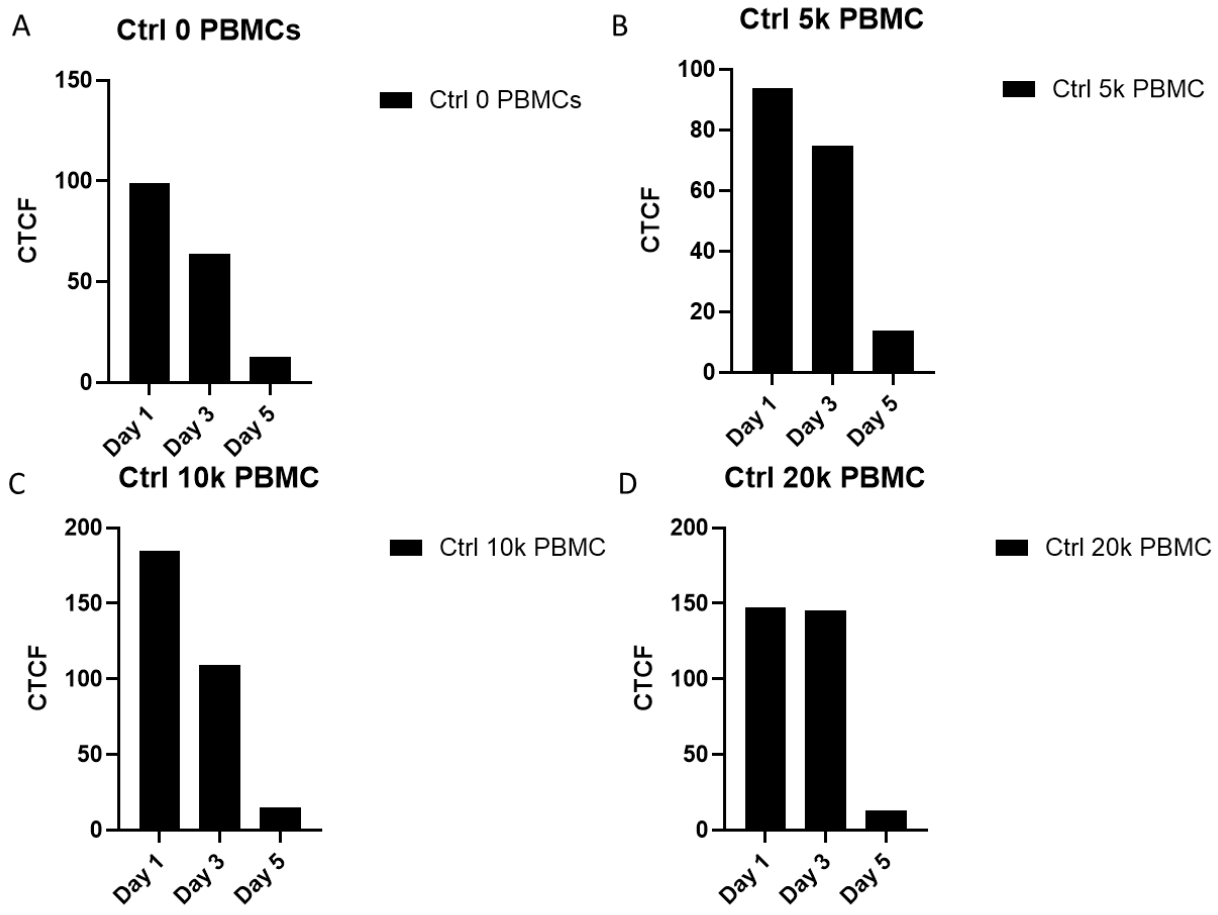

Figure 7 0μM ADU-S100(Ctrl) Co-culture: Corrected total fluorescence measurement of 10k DIPG-36 cell line at Day 1, Day 3, and Day 5 after treatment with PBS and A no PBMCs, B 5k PBMCs C10k PBMCs and D 20k PBMCS

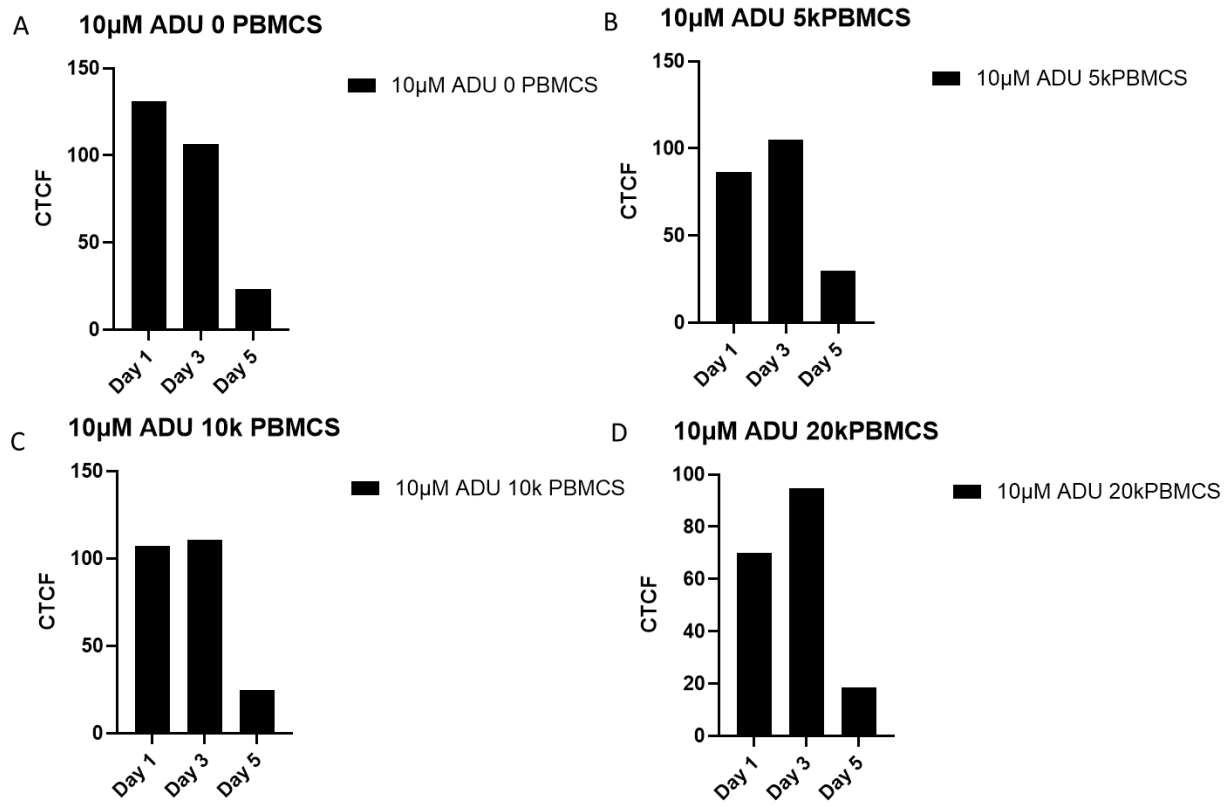

Figure 8 10μM ADU-S100 Co-culture: Corrected total fluorescence measurement of 10k DIPG-36 cell line at Day 1, Day 3, and Day 5 after treatment with 10μM ADU-S100 and A no PBMCs, B 5k PBMCs C10k PBMCs and D 20k PBMCS

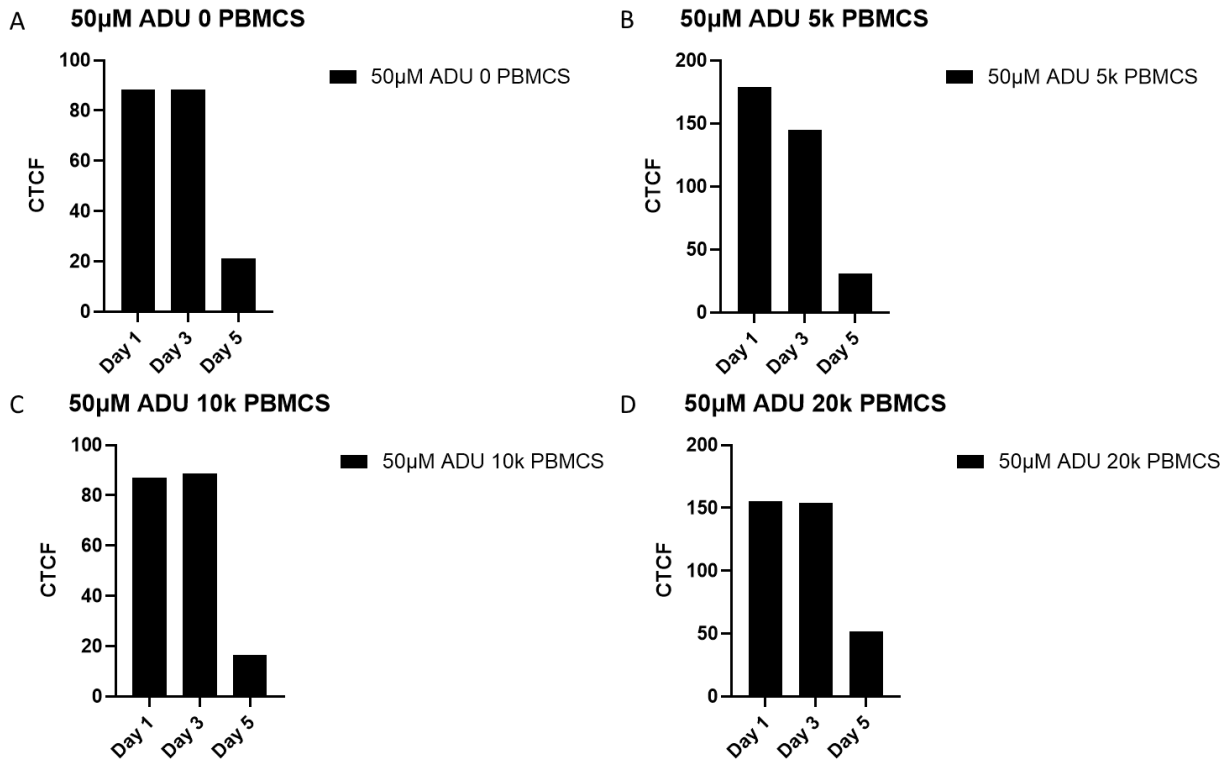

Figure 9 50µM ADU-S100 Co Culture results: Corrected total fluorescence measurement of 10k DIPG-36 cell line at Day 1, Day 3, and Day 5 after treatment with 50µM ADU-S100 and A no PBMCs, B 5k PBMCs C10k PBMCs and D 20k PBMCS

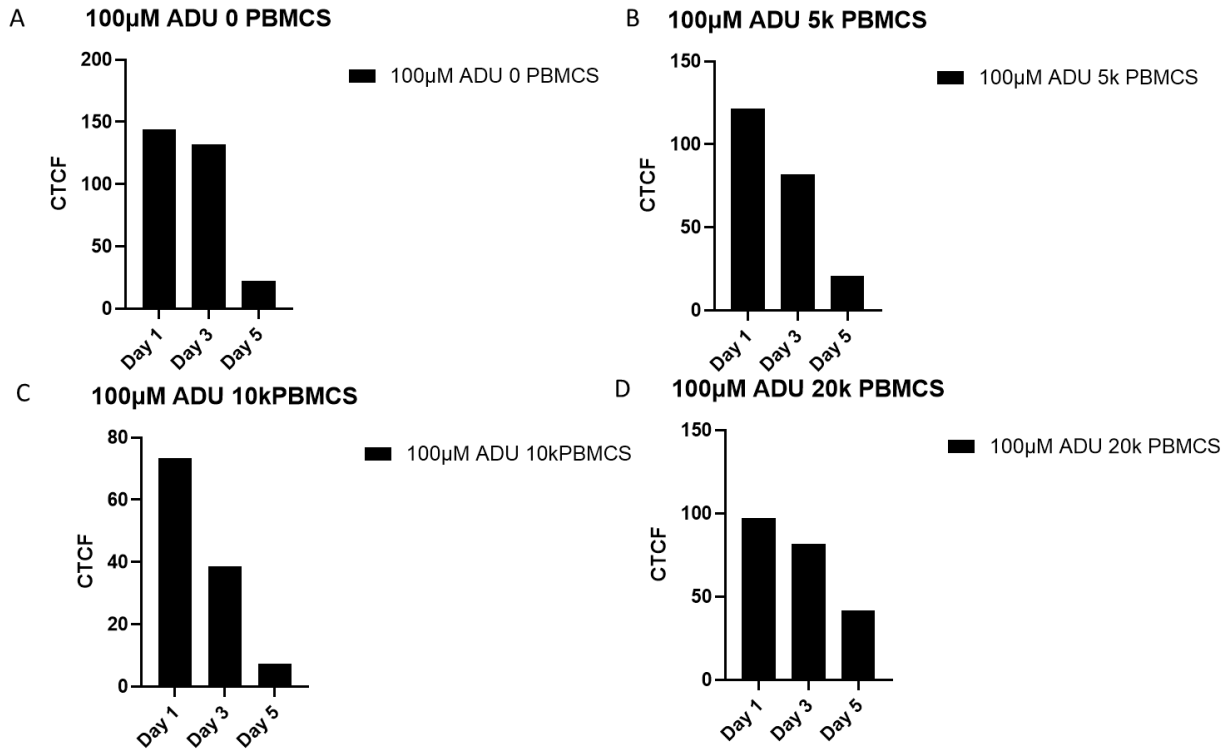

Figure 10 100µM ADU-S100 Co-culture: Corrected total fluorescence measurement of 10k DIPG-36 cell line at Day 1, Day 3, and Day 5 after treatment with 100µM ADU-S100 and A no PBMCs, B 5k PBMCs C10k PBMCs and D 20k PBMCS

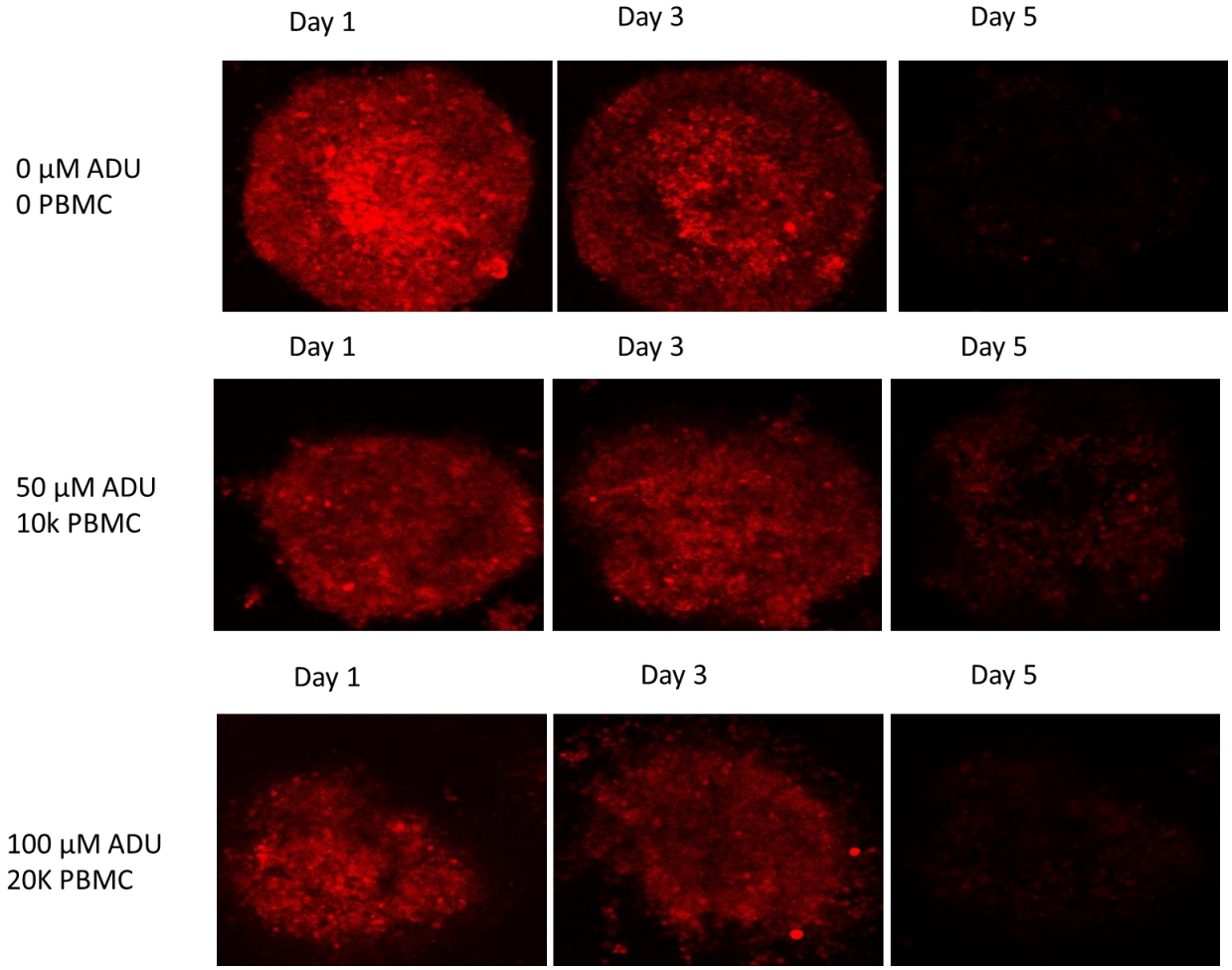

Figure 11 IF imaging of DIPG-36 cells in co-culture: Immunofluorescent images of DIPG-36 cells during co-culture experiment 0µM ADU-S100 and 0 PBMCs on Day1, Day 3, and Day 5. 50µM ADU-S100 and 10k PBMCs' on day 1, day 3, and day 5, and 100µM ADU-S100 and 20K PBMCs on Day 1, Day 3, and Day 5. Red dye shown is mCherry construct that DIPG-36 cells express post lentiviral transfection. Quantitative results for these can be seen in figures 7-10.

***In Vivo* Model**:

To establish an *in vivo* model for future studies, we used KPD mouse cell lines, which harbor the H3K27M mutation along with loss-of-function p53 and D842V. PDGFRA mutations (previously described by our collaborators (21)), were implanted intracranially into the striatum. Although this implantation location does not fully replicate the clinical presentation of midline gliomas, it provides a valuable starting point for preclinical therapeutic testing. 51 days after tumor implantation, brains were harvested and fixed in formalin before being sectioned and stained for the H3K27M mutation (Figure 12A). In figure 12D, we show that the KPD cell lines express H3K27M *in vitro*. In Figure 12B we show the staining of H3K27M *in vivo* in red localized at the nucleus as demonstrated by the co-localization with the nuclear stain DAPI. We also show hematoxylin and eosin staining of the brains to demonstrate pathological signs of tumorigenesis. This data shows that the KPD models can grow in the striatum of mouse brains and may be a useful model for future studies.

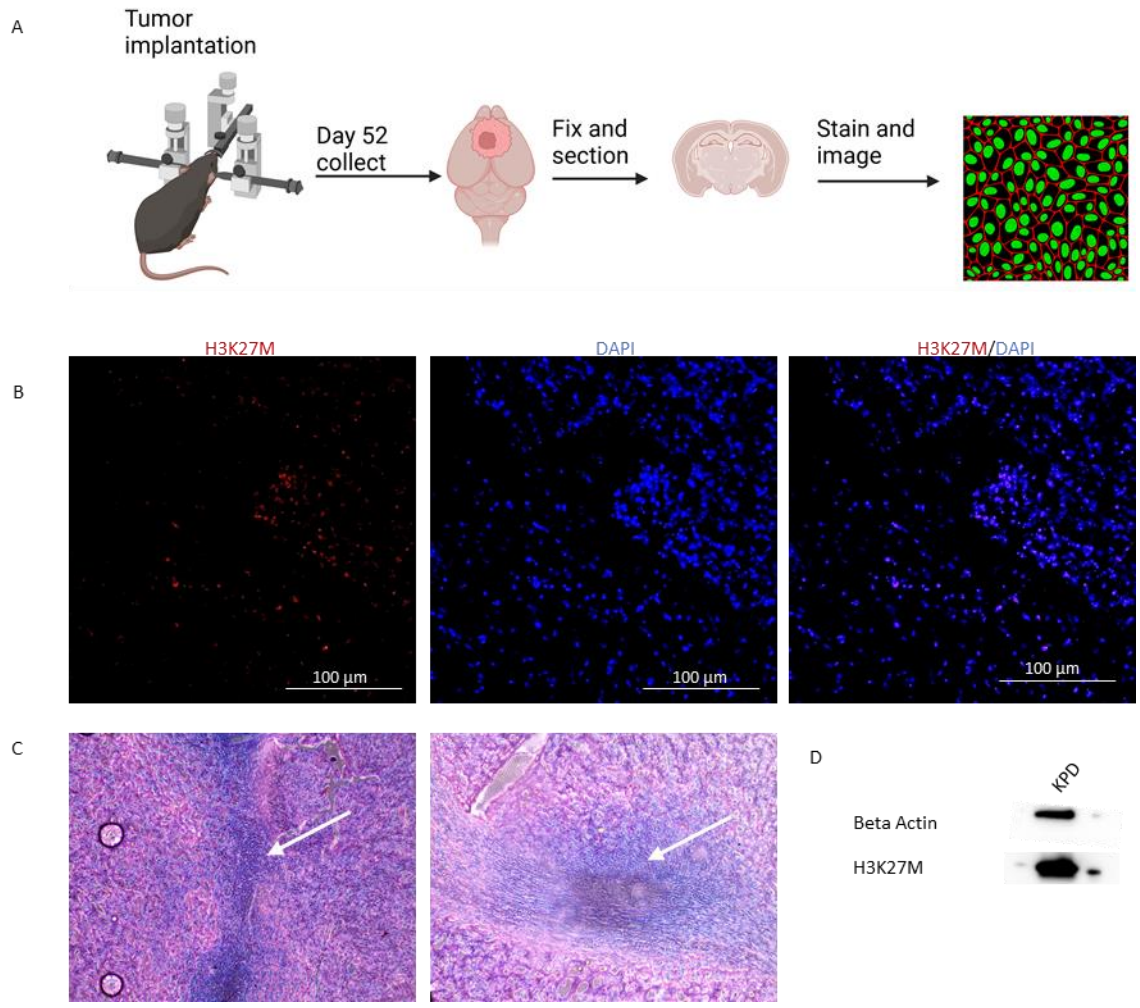

Figure 12 *In vivo* model and tumor staining: A schematic of *in vivo* experimental plan. Created with Biorender. B H3K27M staining of brain samples 52 days post tumor implantation. H3K27M in red and DAPI in blue. C hematoxylin and Eosin Staining with arrows pointing to areas that are pathologically similar to tumor tissue. D H3K27M protein levels of the KPD cell lines *in-vitro* with β-actin as a loading control.

Chapter 4: Discussion and Conclusion:

pHGG is a heterogeneous class of cancer that despite the rapid acceleration in cancer research since the millennia have been left without effective treatments. We hypothesized that by targeting the cGAS-STING pathway we could induce a type I interferon response and sequential immune mediated cell death that would allow us to turn these immunologically cold tumors hot (14). Excitingly, we observed ADU-S100 successfully agonize the cGAS-STING pathway in DIPG-36 cells, and a reduction in cell viability in the DIPG-4 cell line. Both of these results have the potential to lead to avenues for therapeutic use of ADU-S100, or other cGAS-STING agonists.

ADU-S100 successfully agonizes the STING pathway in DIPG-36:

In this study, we demonstrate that the cGAS-STING pathway can be successfully activated by ADU-S100 in DIPG-36 cells, while DIPG-4 and KNS-42 cells did not show similar activation. Typically, STING protein undergoes ubiquitination and subsequent degradation via autophagy post-activation to prevent overstimulation from type I interferon responses (25,26). Consistent with this, we observed a marked reduction of STING protein in KNS-42 and DIPG-4 cell lines following ADU-S100 treatment, although no cytokine secretion (CCL5, CXCL10) was detected at the 24-hour time point. A potential explanation could be insufficient time for effective ADU-S100 uptake or incomplete downstream STING activation within this period. Additionally, our group has previously observed STING protein reduction without corresponding canonical pathway activation in GBM cell lines (unpublished data Lawler lab STING group), suggesting the possibility of downstream signaling dysregulation in certain glioma cells. In contrast, DIPG-

36 cells maintained stable STING levels post-treatment, consistent with robust and measurable secretion of inflammatory cytokines (Figure 6).

The co-culture experiments were inconclusive, largely due to issues maintaining spheroid stability. Canonically CCL5 should recruit immune cells by binding C-C chemokine receptor type 5 (CCR5) a receptor on the surface of T cells, monocytes, macrophages and Eosinophils and attracting them towards the site of insult (27). CXCL10 acts similarly to CCL5 binding the C-X-C motif chemokine receptor 3 (CXCR3) receptor attracting T cells, natural killer (NK) cells, dendritic cells, macrophages, and B cells (28). PBMCs are a diverse population of immune cells that circulate through the blood consisting primarily of T cells, B cells, Nk cells, monocytes and dendritic cells. Hence if CCL5 and CXCL10 are being excreted by DIPG-36 cells post agonization with cGAS-STING agonist ADU-S100 there should be an activating effect and subsequent immune mediated cell death. In these studies we did not observe that and plan to optimize this experiment in the future. Future experiments will specifically optimize PBMC ratios and media composition, alongside complementary viability assays, to robustly evaluate immune-mediated tumor cytotoxicity.

cGAS as an activator of senescence possible explanation for decrease in viability:

Of special interest in this study are the results presented in Figure 1C, where we observed a significant reduction in cell viability in DIPG-4 cells following treatment with ADU-S100, independent of irradiation. The assay used, Promega's CellTiter-Glo, which quantifies Adenosine Triphosphate (ATP) levels as a proxy for cellular viability (30). Importantly, changes in ATP do not necessarily directly correlate with cell death but can also indicate decreased metabolic

activity resulting from altered cellular processes. Previous literature has identified a link between cGAS activity and cellular senescence, particularly in mouse embryonic fibroblast (MEF) models. Notably, cGAS knockout MEFs demonstrate an increased propensity toward senescence compared to wild-type counterparts (31). Mechanistically, cGAS is thought to drive senescence through autocrine signaling mediated by cytosolic chromatin fragments produced by DNA damage (32,33). Additionally, the generation of cytosolic chromatin fragments is known to increase following radiation-induced DNA damage (34).

ADU-S100 directly agonizes the cGAS-STING pathway by acting as cGAMP, effectively bypassing the need for initial cGAS recognition of extranuclear DNA. Given that DIPG-4 cells express cGAS, it is possible that treatment with ADU-S100, particularly in the presence of radiation-induced cytosolic DNA fragments, could stimulate a senescent phenotype via autocrine cGAS-STING activation. Such senescence would significantly impair cellular metabolism, replication, and consequently ATP production. We therefore hypothesize that the observed reduction in ATP levels in DIPG-4 cells (Figure 1C) might reflect entry into cellular senescence rather than direct cytotoxicity.

Supporting this hypothesis, we observed similar viability reductions in Human Cerebral Microvascular Endothelial Cells (HCMECs) treated with ADU-S100 and radiation. Our laboratory's preliminary unpublished observations have demonstrated an intact and functional cGAS-STING pathway in HCMECs (unpublished data, Lawler Lab STING group), further supporting the potential connection between pathway activation and senescence. Notably, while all tested cell lines express cGAS, only DIPG-4 and HCMEC cell lines exhibited significant

viability reductions post-treatment, highlighting possible cell-type-specific responses and sensitivities.

To conclusively determine whether senescence underlies the reduction in ATP observed in DIPG-4 cells, future experiments must directly measure senescence markers such as β-galactosidase activity (β-Gal staining). Additionally, performing complementary viability assays, such as trypan blue exclusion, will help differentiate between senescent and apoptotic or necrotic outcomes following ADU-S100 treatment. These experiments are critical to validating our senescence hypothesis and guiding subsequent therapeutic strategies involving cGAS-STING agonists.

Generation of a DMG mouse model that mirrors human disease:

Lastly, a significant achievement of this study was the successful establishment of a DMG mouse model that recapitulates key features of human disease, specifically the presence of the clinically relevant H3K27M mutation. The H3K27M mutation, characterized by a lysine-to-methionine substitution at position 27 of histone H3, plays a pivotal role in the pathogenesis and prognosis of DMG tumors. Our mouse model demonstrated robust expression of this mutant histone *in vivo*, with clear nuclear localization confirmed by immunofluorescence staining (Figure 12a). This nuclear localization aligns with previously described clinical and preclinical observations, providing confidence that our mouse model closely mirrors critical molecular aspects of the human condition.

Histopathological analysis further validated our model's fidelity. Hematoxylin and eosin staining revealed regions of increased cellular density, abnormal cellular architecture, and atypical nuclear morphology, consistent with the characteristic histology of high-grade gliomas described extensively in literature (21). Independent evaluation by a clinician in our laboratory helped to confirm observed histological features are indicative of tumor formation, reinforcing our model's relevance for preclinical testing.

Establishing reliable animal models of DMG is crucial given the aggressive nature and limited therapeutic options currently available for this disease. However, while the establishment of tumors via intracranial injection into the striatum was methodologically advantageous and reliably facilitated initial tumor growth, we acknowledge that this anatomical site does not fully replicate the midline tumor locations typically observed in pediatric DMG patients, such as the pons or thalamus. Tumor location critically influences multiple biological processes, including tumor progression, interaction with the surrounding brain microenvironment, immune infiltration patterns, and drug penetrance. Thus, the anatomical differences between the striatal implantation and clinically relevant midline structures potentially limit the direct translational applicability of our findings.

Despite these limitations, our established mouse model provides a robust and valuable initial platform for evaluating therapeutic efficacy and understanding tumor biology. Future studies should prioritize transitioning to orthotopic implantation into midline anatomical regions such as the pons or midbrain. Achieving tumor growth in these clinically relevant regions would greatly enhance the translational value of the model, providing more accurate insights into tumor

biology, immune interactions, and therapeutic responses. Additionally, comparing tumor progression, immune cell infiltration, and treatment efficacy between striatal and midline locations could yield critical insights into anatomical influences on DMG pathogenesis and treatment.

Limitations of the Study:

These studies are exploratory in nature and many of them need to be repeated, specifically the CXCL10 and CCL5 ELISA, and the PBMC co-culture. Significant further optimization of the co-culture protocol is required to prevent spheroid collapse and ensure consistent cell viability and accurate assessment of immune-mediated cytotoxicity. Adjustments in number of cells and media composition should be optimized for both tumor cell viability and PBMC long term viability if this assay is to be a good representation of immune mediated cell death.

It is prudent to note as well that in our hands the DIPG-36 and DIPG-4 cell lines are difficult to work with. These cell lines frequently exhibit morphological changes or spontaneous cell death during routine passaging, independent of external manipulations. Additionally, their relatively slow doubling time (approximately four days) limits passaging frequency and complicates high-throughput experimental approaches. They are not conducive to high throughput experiments because of this and have been a major hurdle for this work.

Cancer cell lines are not representative of the tumor microenvironment, and as such more experiments are needed to better understand how surrounding cells such as microglia, may react to ADU-S100 as well.

The mouse model used in this study was also implanted in the striatum of the brain closer to the forebrain instead of a more physiologically relevant sight for implantation along the midbrain or into the pons. This was done in this study to allow us to establish that the tumors would grow in the brain and retain their mutational profile before dedicating resources to redesigning our established model. In future studies, the establishment of a more physiologically relevant tumor model through orthotopic implantation into midline regions such as the pons or midbrain would significantly enhance clinical relevance and translational potential.

Future Directions:

In summary, ADU-S100 agonizes the cGAS-STING pathway in the DIPG-36 cell lines, causes a reduction in ATP 72 hours post treatment in the DIPG-4 cell line, and we were able to successfully implant a DMG like mouse tumor into a mouse model. To further test our hypothesis, first proteomics and genomic analysis should be performed to elucidate changes in the proteome and gene expression between both DIPG-4, DIPG-36 and KNS-42 cell lines. Doing this allows for better understanding of mutational burden and heterogeneity in the proteome that could be responsible for the differences in outcomes. DIPG-4 cell lines should be stained for β-Gal (Yang Hui et al.) a senescence marker post ADU-S100 treatment and a simple trypan blue readout after treatment with ADU-S100 to elucidate the mechanism behind ADU-S100 mediated reduction in ATP seen in our cell titer glo assay. In the case of KNS-42 cells we do see a reduction in STING 24 hours after treatment with ADU-S100 but we see no cytokine response suggesting some downstream protein disruption. Further investigation into what is causing the juxtaposition between the protein and cytokine response is needed.

Long term, understanding if our current *in vivo* model is a responder cell line to ADU-S100 by repeating these western blots, ELISAs and an optimized co-culture. If it is not using a mouse cell line with a different mutational burden that does respond would be pertinent to understanding how the tumor and tumor microenvironment reacts to ADU-S100 and if we see similar results to what we saw in GBM.

Finally, exploring combination therapies with ADU-S100 and immune checkpoint blockade warrants investigation, as synergistically targeting both innate and adaptive immune responses could substantially improve therapeutic outcomes. Agonizing the innate immune system alone may not be enough for immune mediated cell death but in combination with other immunotherapies may prove exponentially effective.

References:

1. Hu, Jiuan. "Role of H3.3-G34R Mutation in Pediatric High-Grade Glioma." *Alex's Lemonade Stand Foundation for Childhood Cancer*, 27 Aug. 2021, www.alexslemonade.org/project/role-h33-g34r-mutation-pediatric-high-grade-glioma.
2. Vallero, Stefano Gabriele, et al. "Pediatric diffuse midline glioma H3K27- altered: A complex clinical and biological landscape behind a neatly defined tumor type." *Frontiers in Oncology*, vol. 12, 16 Jan. 2023, https://doi.org/10.3389/fonc.2022.1082062.
3. Al Sharie, Sarah, et al. "Decoding diffuse midline gliomas: A comprehensive review of pathogenesis, diagnosis and treatment." *Cancers*, vol. 15, no. 19, 6 Oct. 2023, p. 4869, https://doi.org/10.3390/cancers15194869.
4. Crowell, Cameron, et al. "Systematic review of diffuse hemispheric glioma, H3 G34-mutant: Outcomes and associated clinical factors." *Neuro-Oncology Advances*, vol. 4, no. 1, 1 Jan. 2022, https://doi.org/10.1093/noajnl/vdac133.
5. Himes, Benjamin T., et al. "Treatment strategies in diffuse midline gliomas with the H3K27M mutation: The role of convection-enhanced delivery in overcoming anatomic challenges." *Frontiers in Oncology*, vol. 9, 8 Feb. 2019, https://doi.org/10.3389/fonc.2019.00031.
6. Pfister, Stefan M., et al. "A summary of the inaugural who classification of pediatric tumors: Transitioning from the optical into the molecular era." *Cancer Discovery*, vol. 12, no. 2, 17 Dec. 2021, pp. 331–355, https://doi.org/10.1158/2159-8290.cd-21-1094.
7. Bender, Sebastian, et al. "Reduced h3k27me3 and DNA hypomethylation are major drivers of gene expression in K27M mutant pediatric high-grade gliomas." *Cancer Cell*, vol. 24, no. 5, Nov. 2013, pp. 660–672, https://doi.org/10.1016/j.ccr.2013.10.006.
8. Nguyen, Anthony V., et al. "H3G34-mutant gliomas—a review of molecular pathogenesis and therapeutic options." *Biomedicines*, vol. 11, no. 7, 15 July 2023, p. 2002, https://doi.org/10.3390/biomedicines11072002.
9. "Home." *Cellosaurus*, 22 Sept. 2022, www.cellosaurus.org/CVCL_C1N5.
10. "Home." *Cellosaurus*, Mar. 2017, www.cellosaurus.org/CVCL_IT39.
11. Philippova, Julia, et al. "GD2-targeting therapy: A comparative analysis of approaches and promising directions." *Frontiers in Immunology*, vol. 15, 15 Mar. 2024, https://doi.org/10.3389/fimmu.2024.1371345.
12. "Anti-GD2 car T cells are potent in H3-K27M+ diffuse midline gliomas." *Cancer Discovery*, vol. 8, no. 6, 31 May 2018, pp. 672–672, https://doi.org/10.1158/2159-8290.cd-rw2018-070.
13. Monje, Michelle, et al. "Intravenous and intracranial GD2-car T cells for H3K27M+ diffuse midline gliomas." *Nature*, vol. 637, no. 8046, 13 Nov. 2024, pp. 708–715, https://doi.org/10.1038/s41586-024-08171-9.
14. Persson, Mika L, et al. "The intrinsic and microenvironmental features of diffuse midline glioma: Implications for the development of effective immunotherapeutic treatment strategies." *Neuro-Oncology*, vol. 24, no. 9, 27 Apr. 2022, pp. 1408–1422, https://doi.org/10.1093/neuonc/noac117.
15. Haase, Santiago, et al. "H3.3-G34 mutations impair DNA repair and promote CGAS/sting-mediated immune responses in pediatric high-grade glioma models." *Journal of Clinical Investigation*, vol. 132, no. 22, 15 Nov. 2022, https://doi.org/10.1172/jci154229.

16. Barrat, Franck J., et al. “Importance of nucleic acid recognition in inflammation and autoimmunity.” *Annual Review of Medicine*, vol. 67, no. 1, 2 Nov. 2015, pp. 323–336, https://doi.org/10.1146/annurev-med-052814-023338.
17. Samson, Natasha, and Andrea Ablasser. “The CGAS–sting pathway and cancer.” *Nature Cancer*, vol. 3, no. 12, 12 Dec. 2022, pp. 1452–1463, https://doi.org/10.1038/s43018-022-00468-w.
18. Decout, Alexiane, et al. “The CGAS–sting pathway as a therapeutic target in inflammatory diseases.” *Nature Reviews Immunology*, vol. 21, no. 9, 8 Apr. 2021, pp. 548–569, https://doi.org/10.1038/s41577-021-00524-z.
19. Han Y, Guo Z, Jiang L, Li X, Chen J, Ouyang L, Li Y, Wang X. CXCL10 and CCL5 as feasible biomarkers for immunotherapy of homologous recombination deficient ovarian cancer. Am J Cancer Res. 2023 May 15;13(5):1904-1922. PMID: 37293164; PMCID: PMC10244116.
20. Xiao, G et al. “NF-kappaB-inducing kinase regulates the processing of NF-kappaB2 p100.” Molecular cell vol. 7,2 (2001): 401-9. doi:10.1016/s1097-2765(01)00187-3
21. McNicholas, Michael, et al. “A Compendium of Syngeneic, Transplantable Pediatric High-Grade Glioma Models Reveals Subtype-Specific Therapeutic Vulnerabilities .” *Cancer Discovery*, vol. 13, no. 7, 1 July 2023, pp. 1592–1615.
22. Berger, Gilles, et al. *Sting Activation Promotes Robust Immune Response and NK Cell-Mediated Tumor Regression in Glioblastoma Models*, 1 Mar. 2022, https://doi.org/10.1101/2022.02.28.481908.
23. Jiang, Minlin, et al. “CGAS-Sting, an important pathway in cancer immunotherapy.” *Journal of Hematology & Oncology*, vol. 13, no. 1, 22 June 2020, https://doi.org/10.1186/s13045-020-00916-z.
24. Mutlu, Merve, et al. “Small molecule induced sting degradation facilitated by the HECT ligase herc4.” *Nature Communications*, vol. 15, no. 1, 29 May 2024, https://doi.org/10.1038/s41467-024-48922-w.
25. Tu, Xintao, et al. “Interruption of post-golgi sting trafficking activates tonic interferon signaling.” *Nature Communications*, vol. 13, no. 1, 15 Nov. 2022, https://doi.org/10.1038/s41467-022-33765-0.
26. Prabakaran, Thaneas, et al. “Attenuation of cGAS-STING signaling is mediated by a p62/SQSTM1-dependent autophagy pathway activated by TBK1.” *The EMBO Journal*, vol. 37, no. 8, Mar. 2018, https://doi.org/10.15252/embj.201797858.
27. Melese, Etienne S., et al. “CCL5 production in lung cancer cells leads to an altered immune microenvironment and promotes tumor development.” *OncoImmunology*, vol. 11, no. 1, 30 Dec. 2021, https://doi.org/10.1080/2162402x.2021.2010905.
28. LIU, MINGLI, et al. “The emerging role of CXCL10 in cancer (review).” *Oncology Letters*, vol. 2, no. 4, 9 May 2011, pp. 583–589, https://doi.org/10.3892/ol.2011.300.
29. Kleiveland CR. Peripheral Blood Mononuclear Cells. In: Verhoeckx K, Cotter P, López-Expósito I, et al., editors. The Impact of Food Bioactives on Health: in vitro and ex vivo models [Internet]. Cham (CH): Springer; 2015. Chapter 15. Available from: https://www.ncbi.nlm.nih.gov/books/NBK500157/ doi: 10.1007/978-3-319-16104-4_15
30. “CellTiter-Glo® Luminescent Cell Viability Assay Technical Bulletin.” *CellTiter-Glo® Luminescent Cell Viability Assay Protocol*, Promega, www.promega.com/resources/protocols/technical-bulletins/0/celltiter-glo-luminescent-cell-viability-assay-protocol/. Accessed 27 Mar. 2025.

31. Yang, Hui, et al. “CGAS is essential for cellular senescence.” *Proceedings of the National Academy of Sciences*, vol. 114, no. 23, 22 May 2017, https://doi.org/10.1073/pnas.1705499114.
32. Glück, Selene, et al. “Innate immune sensing of cytosolic chromatin fragments through cgas promotes senescence.” *Nature Cell Biology*, vol. 19, no. 9, 31 July 2017, pp. 1061–1070, https://doi.org/10.1038/ncb3586.
33. Freyter, Benjamin M., et al. “Nuclear fragility in radiation-induced senescence: Blebs and tubes visualized by 3D electron microscopy.” *Cells*, vol. 11, no. 2, 13 Jan. 2022, p. 273, https://doi.org/10.3390/cells11020273.
34. Yu, Le, and Pengda Liu. “CGAS/sting signalling pathway in senescence and oncogenesis.” *Seminars in Cancer Biology*, vol. 106–107, Nov. 2024, pp. 87–102, https://doi.org/10.1016/j.semcancer.2024.08.007.